Symmetry effects on nonlocal electron-phonon coupling in organic semiconductors

Yuan Li, Yuanping Yi, Veaceslav Coropceanu, and Jean-Luc Brédas

Symmetry effects on nonlocal electron-phonon coupling in organic semiconductors

Yuan Li,[1,2] Yuanping Yi,[1] Veaceslav Coropceanu,[1,*] and Jean-Luc Brédas[1,†]

[1]*School of Chemistry and Biochemistry and Center for Organic Photonics and Electronics,*
Georgia Institute of Technology, 901 Atlantic Drive NW, Atlanta, Georgia 30332-0400
[2]*Department of Physics, Southeast University, Nanjing 211189, China*
(Dated: May 18, 2012)

The electronic and electrical properties of crystalline organic semiconductors, such as the dispersions of the electronic bands and the dependence of charge-carrier mobility on temperature, are greatly impacted by the nonlocal electron-phonon interactions associated with intermolecular lattice vibrations. Here, we present a theoretical description that underlines that these properties vary differently as a function of the symmetry of the nonlocal electron-phonon coupling mechanism. The electron-phonon coupling patterns in real space are seen to have direct and significant impact on the interactions in reciprocal space. Our findings demonstrate the importance of aspects that are usually missing in current transport models. Importantly, an adequate description of the electronic and charge-transport properties of organic semiconductors requires that the models take into account both antisymmetric and symmetric contributions to the nonlocal electron-phonon coupling mechanism.

I.   INTRODUCTION

While organic molecular semiconductors have been actively investigated for several decades, reaching a complete understanding of their charge-transport mechanism still poses a major challenge. Until recently, it was commonly assumed that: (i) at low temperatures, these systems could exhibit a conventional band-like behavior with the mobility decreasing in a power-law fashion with increasing temperature; and, (ii) at high temperatures, as a result of strong polaron localization effects (band narrowing), the motion of the carriers could be described as a sequence of uncorrelated hops, with the mobility showing an Arrhenius-like (activated) temperature dependence[1].

Two major electron-phonon (e-ph) coupling mechanisms can be distinguished in the framework of a simple tight-binding description of organic semiconductors. The first comes from the modulation by vibrations of the site energy, ε_n (local or Holstein-type[2,3] e-ph coupling). The second mechanism is due to the dependence of the transfer integral, t_{mn}, on the distances between adjacent molecules and their relative orientations (nonlocal or Peierls-type[3,4] e-ph coupling). The band-to-hopping crossover of the charge-transport mechanism is generally associated with a Holstein-type polaron coupling. However, the results of extensive experimental and theoretical studies have shown that, in most organic systems of current interest such as oligoacenes and their derivatives, the polaron binding energy (or relaxation energy) due to local coupling is comparable to or even (much) smaller than the width of the conduction and valence bands[1,5,6]. In addition, the largest part of the polaron binding energy arises from high-frequency *intra*molecular vibrations whose excited levels are thermally inaccessible even at room temperature. Therefore, a Holstein-type mechanism taken alone cannot provide a comprehensive description of the charge-transport properties of organic semiconductors.

On the other hand, there is currently a growing consensus that the nonlocal e-ph coupling mechanism plays an important or even dominant role in organic semiconductors[1,7–19]. Although a detailed quantum-chemical investigation of the nonlocal e-ph coupling has been performed to date only for a few systems[14–16], the results underline that the nonlocal e-ph coupling mechanism can be very complex and, depending on the nature of the relevant phonon modes, can result in different dynamical disorder patterns. The latter aspect is largely overlooked in most current theoretical studies since these are commonly based on models that consider only a single specific dynamical disorder pattern. In this work, we show that, as a function of their symmetry, various contributions to the nonlocal e-ph coupling mechanism can affect *in remarkably different ways* the electronic spectrum of organic semiconductors and, consequently, their charge-transport as well as spectroscopic properties.

II.   MODEL

We illustrate the problem by employing a Su-Schrieffer-Heeger (SSH)-type Hamiltonian[20]:

$$H = -\sum_n t_{n,n+1} \left(a_n^\dagger a_{n+1} + h.c.\right) + \sum_{nj} \frac{\hbar\omega_j}{2} \left(u_{nj}^2 + p_{nj}^2\right). \tag{1}$$

Here $a_n^\dagger$ and a_n denote the creation and annihilation operators for an electron at site n; $t_{n,n+1}$ represents the transfer integral between adjacent molecules; ω_j, u_{nj} and p_{nj} denote, respectively, the frequency and the dimensionless coordinate and momentum of the jth vibration mode associated with site n. The nonlocal e-ph coupling is obtained by expanding the transfer integral in a power series of the molecular displacements:

$$t_{n,n+1} = t^{(0)} + \sum_j \left(v_{nj} u_{nj} + v_{n+1,j} u_{n+1,j}\right) + \cdots, \tag{2}$$

where $t^{(0)}$ is the transfer integral at the equilibrium geometry while $v_{nj} = (\frac{\partial t_{n,n+1}}{\partial u_{nj}})_0$ and $v_{n+1,j} = (\frac{\partial t_{n,n+1}}{\partial u_{n+1,j}})_0$ represent the linear coupling constants. By symmetrizing the vibration coordinates in Eq. (2), the resulting e-ph Hamiltonian can be written as:

$$H_{\text{e-ph}} = \sum_{nj} \left[v_{\text{a}j}\left(u_{nj} - u_{n+1,j}\right) + v_{\text{s}j}\left(u_{nj} + u_{n+1,j}\right)\right]\left(a_n^\dagger a_{n+1} + h.c.\right), \tag{3}$$

where $v_{\text{a}j} = \frac{1}{2}\left(v_{nj} - v_{n+1,j}\right)$ and $v_{\text{s}j} = \frac{1}{2}\left(v_{nj} + v_{n+1,j}\right)$. Following the classification introduced by Lindenberg and co-workers[9], we refer to the $v_{\text{a}j}$ and $v_{\text{s}j}$ terms in Eq. (3) as the *antisymmetric* and *symmetric* nonlocal e-ph coupling mechanism, respectively. The case where a single mode per molecule is considered and the symmetric coupling mechanism is neglected, $v_{\text{s}} = 0$ (i.e., $v_{n+1} = -v_n$), corresponds to the standard SSH model; starting with the work of Munn and Silbey[8], it is the most commonly used model to describe charge transport in organic semiconductors[9,11–13,17,19].
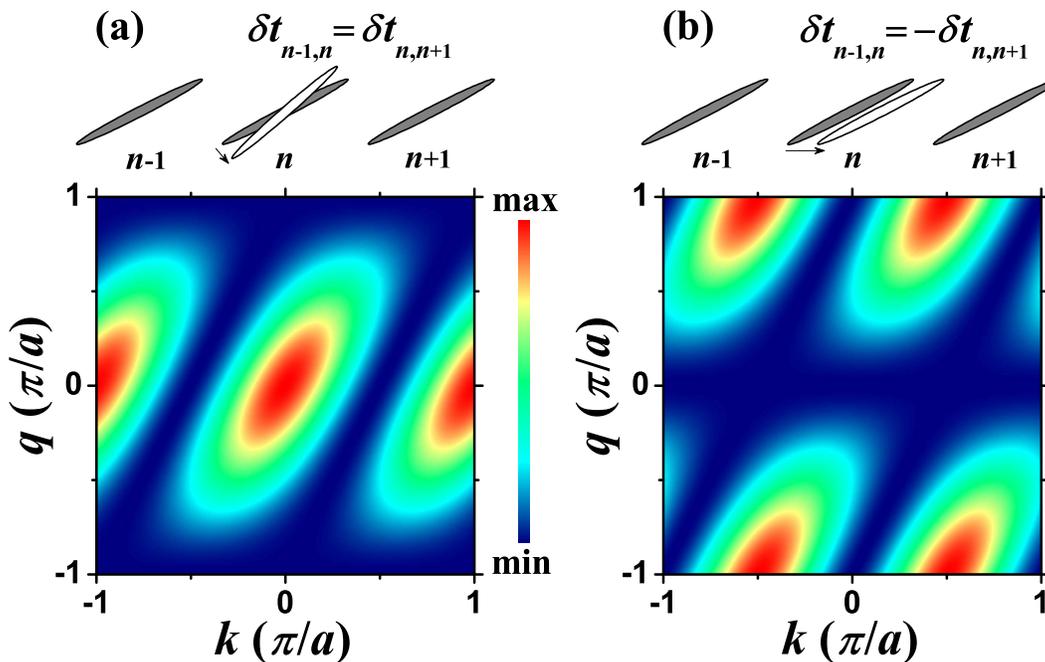
FIG. 1. (Color online) Schematic diagrams of examples of lattice vibrations (top part) and e-ph coupling constants $|v_{kq}|^2$ in reciprocal space (bottom part): (a) symmetric coupling; (b) antisymmetric coupling. Here, $\delta t_{mn} = t_{mn} - t^{(0)}$; k and q are the electron and phonon wave vectors, respectively.

The two coupling mechanisms lead to rather different interaction patterns. In the case of *antisymmetric coupling*, the change in a vibration coordinate u_n results in an increase of the transfer integral between molecule n and its neighbor on one side, and in a decrease of the transfer integral with its neighbor on the other side (see Fig. 1). In the case of *symmetric coupling*, both transfer integrals vary in the same way. It is also instructive to evaluate how these two mechanisms operate in reciprocal space. In the Bloch representation, $H_{\text{e-ph}}$ takes the form:

$$H_{\text{e-ph}} = \sum_{kqj} v_{kqj} Q_{qj} a_k^\dagger a_{k-q}, \tag{4}$$

where

$$v_{kqj} = \frac{2}{\sqrt{N}} \left\{ v_{\text{s}j} \left[\cos(ka) + \cos((k-q)a) \right] + i v_{\text{a}j} \left[\sin(ka) - \sin((k-q)a) \right] \right\}. \tag{5}$$

The antisymmetric and symmetric contributions to $|v_{kq}|^2$ (one mode per molecule) are plotted in Fig. 1. In the case of symmetric coupling, the strongest interactions take place between electrons in states near $k = 0$ and $\pm\frac{\pi}{a}$ (band edges) and long-wavelength phonons; in the case of antisymmetric coupling, the strongest interactions occur between electrons in states near $k = \pm\frac{\pi}{2a}$ (band center) and short-wavelength phonons.

It is convenient to quantify the strength of the dynamical disorder due to e-ph interactions at a given temperature by the variance of the transfer integral:

$$\sigma^2 = \left\langle t_{n,n+1}^2 \right\rangle - \left\langle t_{n,n+1} \right\rangle^2, \tag{6}$$

where $\langle \cdots \rangle$ represents the thermal average over the lattice phonons. In the classical limit ($k_{\text{B}}T \gg \hbar\omega_j$), the variance takes the form:

$$\sigma^2 = 2\left(L_{\text{s}} + L_{\text{a}}\right)k_{\text{B}}T, \tag{7}$$

where $L_{\text{s(a)}} = \sum_j v_{\text{s(a)}j}^2 / \hbar\omega_j$ is the nonlocal relaxation energy. It is important to note that the partition of σ^2 into symmetric and antisymmetric contributions is possible, whether or not a given phonon mode contributes just to one or simultaneously to both nonlocal e-ph coupling mechanisms.
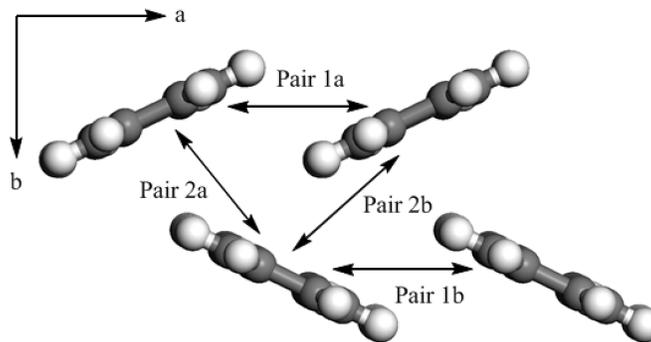
FIG. 2. Sketch of the crystal structure of pentacene and illustration of the molecular pairs presenting the largest transfer integrals and considered in the calculations.

TABLE I. Nonlocal relaxation energies (L_s, L_a, and $L = L_s + L_a$) and transfer integrals $t^{(0)}$ in the pentacene crystal. Here, h and e denote hole and electron, respectively.

	Pair 1a		Pair 1b		Pair 2a		Pair 2b	
	h	e	h	e	h	e	h	e
L_s (meV)	0.70	0.48	0.79	0.54	3.7	1.3	5.3	1.5
L_a (meV)	3.2	2.4	2.4	1.8	5.1	2.6	6.0	3.3
L (meV)	3.9	2.9	3.2	2.3	8.8	3.9	11	4.8
$t^{(0)}$ (meV)	36	-36	37	-37	47	-64	-84	71
$L/t^{(0)}$	0.1	-0.08	0.09	-0.06	0.2	-0.06	-0.1	0.07

III.   ESTIMATES OF ELECTRON-PHONON COUPLING SYMMETRY

The symmetric coupling mechanism has received so far much less attention[9,10] (possibly because it is less intuitive to visualize the corresponding interactions). However, our recent studies[14,15] have demonstrated that this mechanism has a prominent contribution in oligoacenes. Here, we revisit the problem of estimating the e-ph coupling parameters in the specific case of the pentacene crystal.

In contrast to our previous studies[15], we use here a supercell model that allows us to obtain a more accurate description of the e-ph coupling. The geometry optimizations and lattice dynamics of the pentacene crystal have been carried out at the Γ-point based on a supercell that doubles the unit cell along the a axis (see Fig. 2). The calculations were performed with the TINKER program using the OPLS-AA force field[21]. In the course of the geometry optimizations, the cell parameters were fixed at the experimental values[22]. As in our previous study[15], we define $\upsilon_j = \left(\frac{\partial t_{mn}}{\partial Q_j}\right)_0$ as the nonlocal electron-phonon (e-ph) coupling constant of a dimer with respect to the dimensionless normal coordinate Q_j of vibration mode j. It was computed numerically by distorting the crystal along Q_j (with the largest atomic displacement set to 0.01 Å). The transfer integrals for all the generated configurations of dimers, shown in Fig. 2, were evaluated at the semi-empirical Hartree-Fock INDO (intermediate neglect of differential overlap) level. The symmetry of the e-ph coupling for a given vibration mode was determined by considering the sign of υ_j of adjacent dimers along a specific direction. In the case of antisymmetric coupling, υ_j for adjacent dimers are opposite in sign while in the case of symmetric coupling they carry the same sign.

The computed transfer integrals and relaxation energies are listed in Table I (see the supplementary section[23] for more detailed results). The results indicate that the nonlocal relaxation energy can be comparable for the symmetric and antisymmetric mechanisms; depending on the crystal direction, the ratio L_s/L_a is in the range ~ 0.2–0.9. These findings are supported by the results of molecular dynamics simulations in pentacene[24] that show that the absolute value of the correlation function $\frac{\langle \delta t_{n-1,n} \delta t_{n,n+1} \rangle}{\sqrt{\langle \delta t_{n-1,n}^2 \rangle \langle \delta t_{n,n+1}^2 \rangle}}$ ($\delta t_{mn} = t_{mn} - \langle t_{mn} \rangle$) is smaller than 0.25; such a value can be obtained only when symmetric and antisymmetric mechanisms (that present correlation functions of 0.5 and -0.5, respectively) are *both* operational. For the sake of convenience, in the following we use the notation $c = L_{(s)}/L$, where $L = L_s + L_a$. Note that $1 \geq c \geq 0$, where $c = 1$ corresponds to symmetric coupling and $c = 0$ to antisymmetric coupling.

IV.   ELECTRONIC SPECTRAL PROPERTIES

We first consider the e-ph interaction in the static disorder limit for a linear chain of N molecules. In this case, only the electronic part of the Hamiltonian H_e (the first term on the right side of Eq.(1)) is taken into account. The vibration coordinates are assigned random values according to a Gaussian distribution that, at each given temperature T, obeys the statistics of an ensemble of harmonic oscillators with frequency ω. For each set of vibration coordinates, the electronic Hamiltonian of the N-molecule chain is solved numerically assuming open-chain boundary conditions. The electronic density of states (DOS) is computed as:

$$\rho(E) = \left\langle \sum_\nu \delta(E - E_\nu) \right\rangle_{\{u_n\}}, \tag{8}$$

where the E_ν terms correspond to the eigenvalues of H_e and $\langle\cdots\rangle_{\{u_n\}}$ denotes thermal average over a large number of realizations of the lattice configuration $\{u_n\}$. In the calculations, the delta function was replaced by a Lorentzian function with width $0.15\hbar\omega$. In order to investigate the spatial extent of the eigenfunctions, we calculate the energy-resolved localization length, defined here as:

$$\ell^{-1}(E) = \left\langle \sum_\nu \ell_\nu^{-1}\delta(E - E_\nu) / \sum_\nu \delta(E - E_\nu) \right\rangle_{\{u_n\}}, \tag{9}$$

where ℓ_ν is the localization length of the νth eigenfunction calculated according to the Thouless formalism[25]. Fig. 3 collects the $\rho(E)$ and $\ell(E)$ values obtained as an average over 5×10^4 lattice configurations for a chain with $N = 500$ sites, as well as the relevant parameters for oligoacenes. We note that the dominant contribution to the nonlocal relaxation energy in oligoacenes is due to low-energy *inter*molecular modes[15,23]; therefore, in our model calculations, we used a value of $\hbar\omega = 50$ cm^{-1} for the energy of the effective phonon mode. As the transfer integrals $t^{(0)}/\hbar\omega$ in pentacene are in the range $\sim$ 6–14 (see Table I), we considered here an average value of $t^{(0)}/\hbar\omega = 10$ (Ref. 15). In a similar way, the relaxation energy $L/\hbar\omega$ in pentacene is direction-dependent and ranges from 0.4 to 1.8; therefore, we took $L/\hbar\omega = 1$ as a characteristic value for both holes and electrons.

As seen from Fig. 3, in the case of very weak e-ph interactions ($L/\hbar\omega = 0.01$), the shape of $\rho(E)$ for both coupling mechanisms resembles the DOS of an unperturbed one-dimensional system. However, even in this situation, the difference between the antisymmetric and symmetric mechanisms is already evident as the peaks in $\rho(E)$ at the band edges are broader and less intense in the case of symmetric coupling. This is consistent with the fact mentioned above (see Fig. 1) that the impact of symmetric coupling is maximum near the band edges. As the symmetric e-ph coupling increases, the peaks in $\rho(E)$ move towards the band center, become broader and much less intense, and ultimately disappear. In contrast, in the case of the antisymmetric mechanism, as the coupling increases, the peaks in $\rho(E)$ move further away from the band center; while they become broader and less intense as well, they can be distinguished even for very large couplings. We note that the DOS for both mechanisms exhibit a singularity at the band center; this represents a well-known signature of nondiagonal disorder and is related to the chiral symmetry of the system[26,27].

The calculations of $\ell(E)$ reveal that, in the case of symmetric coupling, the states became gradually more localized when going from the band center to the band edges. In the case of antisymmetric coupling, the "band" states ($|E| < 2t^{(0)}$) display a nearly equal (de)localization length (except in the vicinity of $E = 0$). These states are much more extended than the states in the tails outside the band region. The transition between delocalized and localized states, as seen from Fig. 3d, is much sharper than in the case of the symmetric mechanism, Fig. 3b. Thus, $\rho(E)$ and $\ell(E)$ are more strongly affected by the antisymmetric coupling for the inner-band states and by the symmetric coupling at the band edges. When both mechanisms act simultaneously, the results (see Figs. 3e and 3f) can be understood as an approximate superposition of the two contributions.

The concept that large dynamical disorder is required to interpret the charge-transport properties in organic systems has been recently questioned by the results of angle-resolved photoelectron spectroscopy (ARPES) measurements[28–31] that clearly show the existence of well-defined Bloch states in pentacene and rubrene. In order to relate our results to the ARPES data, we computed the single-particle wave-vector resolved spectral function that is proportional to photoemission intensity[32].

$$A(k, E) = \left\langle \frac{1}{N} \sum_{\nu nm} \varphi_\nu(n)\varphi_\nu(m)\cos[k(n-m)a]\delta(E - E_\nu) \right\rangle_{\{u_n\}}. \tag{10}$$
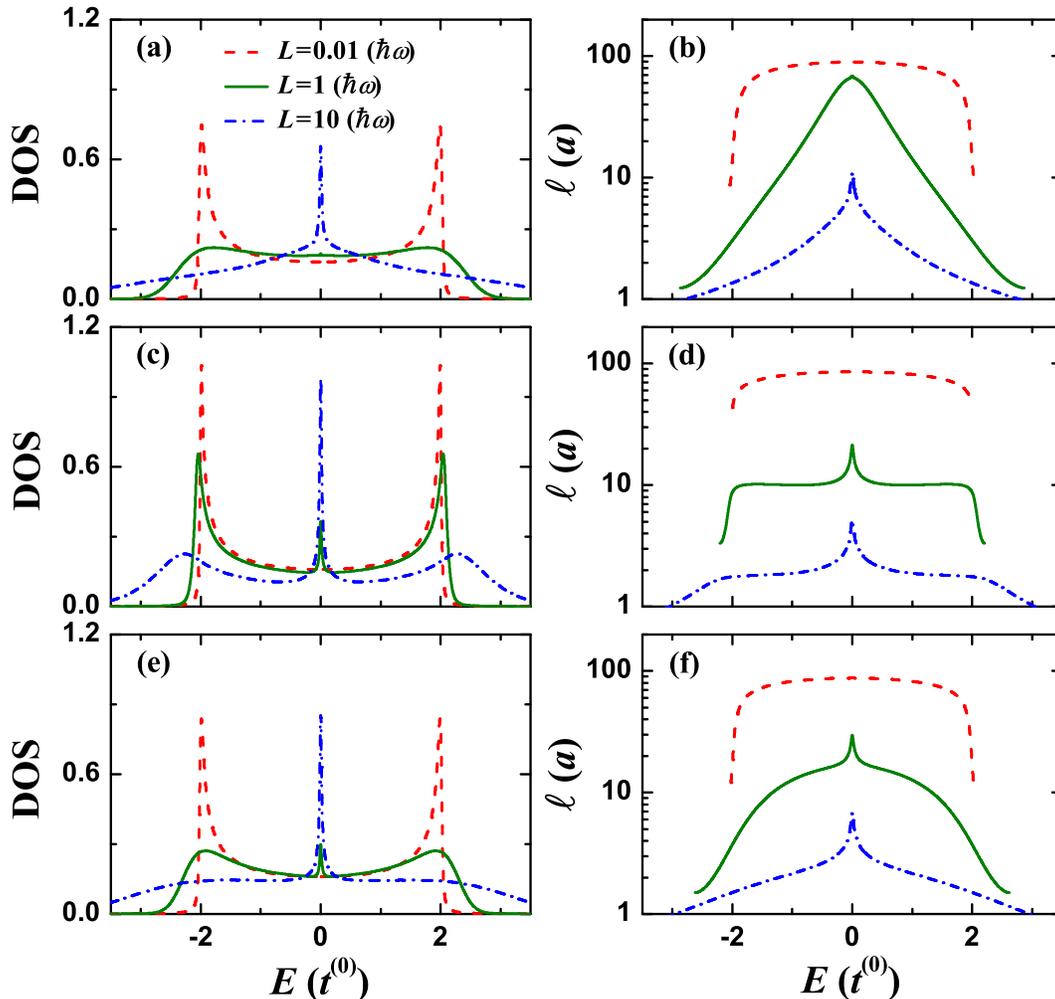
FIG. 3. (Color online) Energy-resolved electronic density of states (in units of $N/t^{(0)}$) and localization length for different e-ph coupling strengths: (a)-(b) symmetric coupling only ($c = 1$); (c)-(d) antisymmetric coupling only ($c = 0$); (e)-(f) both couplings treated on an equal footing ($c = 0.5$). Here, $\hbar\omega = 50$ cm^{-1}, $t^{(0)}/\hbar\omega = 10$, $T = 300$ K, $N = 500$ and the values of L are shown in (a).

This equation is obtained by performing a Fourier transformation to the local density of states:

$$A(n, E) = \sum_{\nu} \varphi_{\nu}^2(n)\,\delta(E - E_{\nu}), \tag{11}$$

where $\varphi_{\nu}(n)$ is the amplitude of the νth eigenfunction on site n. The results are presented in Fig. 4. In the case of very weak e-ph interactions (Figs. 4a, 4d, and 4g), the quasi-particle energy dispersion extracted from $A(k, E)$ is very close to the band energy $E_k = -2t^{(0)}\cos(ka)$. On the other hand, in the case of very strong e-ph couplings (Figs. 4c, 4f, and 4i), the band feature of the energy dispersion has been completely destroyed due to the presence of large dynamical disorder. The results obtained for the pentacene crystal in fact correspond to the case of moderate e-ph couplings (Figs. 4b, 4e, and 4h); in agreement with previous results[12], a well-defined band-like dispersion can be resolved for both mechanisms. However, depending on the nature of the coupling mechanism, there appears a substantial difference in the broadening of the quasi-particle states. For instance, the states around the band edges are much broader for symmetric coupling than antisymmetric coupling. This feature becomes even more evident when the temperature dependence is considered. As shown in Fig. 5, in the case of the symmetric mechanism, the width of the photoemission peak at the Γ-point ($k = 0$) is nearly tripled when the temperature increases from 0 to 300 K. In contrast, the antisymmetric coupling induces only a minor broadening of this peak. We note that, in pentacene, a very significant temperature-induced broadening of the Γ-point peak (and other peaks) is observed[31]. Our present study strongly suggests that these observations can be accounted for by the substantial contribution from the symmetric
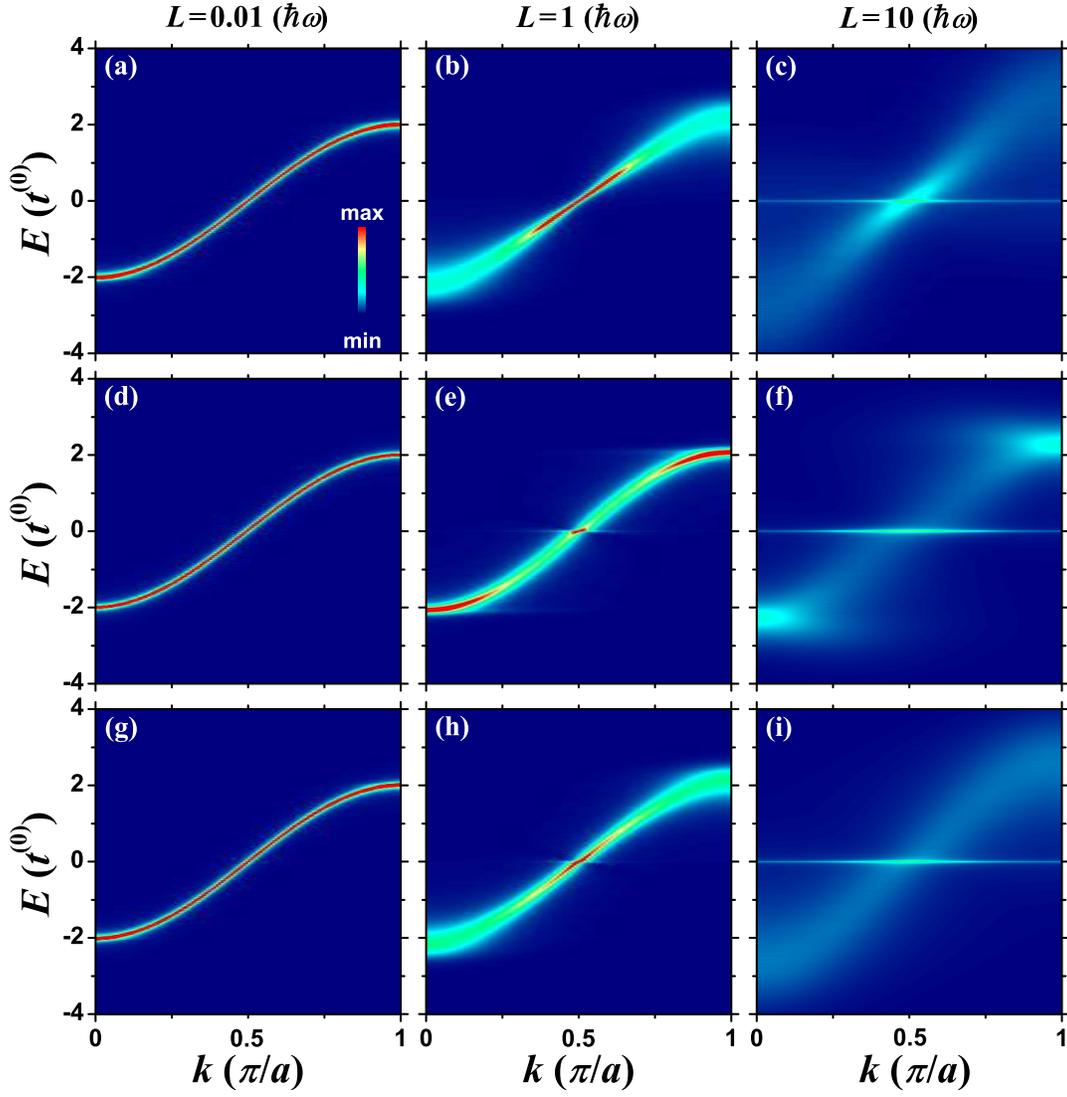
FIG. 4. (Color online) Spectral function $A(k, E)$ for different e-ph coupling strengths. All parameters are the same as in Fig. 3. The values of L are shown on the top of each column sharing the same e-ph coupling strength: (a)-(c) $c = 1$; (d)-(f) $c = 0$; (g)-(i) $c = 0.5$.

nonlocal e-ph coupling mechanism in this system.

The ARPES data for pentacene also indicate that the electronic bands become narrower at higher temperatures[28,31]. However, our calculations indicate that symmetric e-ph coupling, as is the case for antisymmetric coupling[13], leads to an opposite effect, i.e., to band broadening, as shown in Fig. 6. Thus, the observation of band narrowing in this system might be due to coupling to local (Holstein) modes or/and to a temperature-induced lattice expansion[13], resulting in a decrease of $t^{(0)}$. We are currently investigating this effect and the results will be reported elsewhere.

V. CHARGE-TRANSPORT PROPERTIES

We now examine how the antisymmetric and symmetric coupling mechanisms affect charge-carrier mobility. We consider two methods that, while approximate, are well suited to describe charge transport in the pentacene crystal and to explicitly reveal the different impact of the two coupling mechanisms; in the first one, the e-ph interaction is treated as a perturbation (this approach fails for very high temperatures when dynamical disorder becomes significant) while, in the second one, the static description (see Refs. 12 and 17 for earlier applications of this approach to organic semiconductors) used in the previous section is retained.
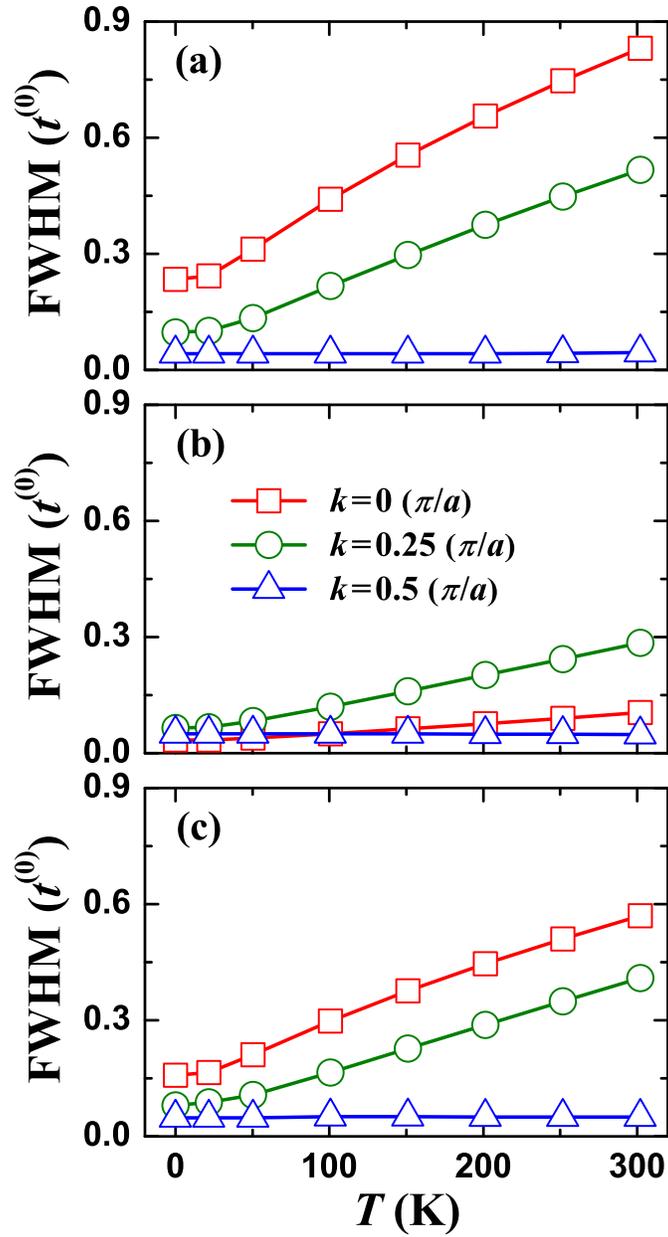
FIG. 5. (Color online) Full width at half maximum (FWHM) of the spectral function for different k values as a function of temperature. Here, $\hbar\omega = 50$ cm^{-1}, $t^{(0)}/\hbar\omega = 10$, $L/\hbar\omega = 1$, $T = 300$ K and $N = 500$ (a) $c = 1$; (b) $c = 0$; (c) $c = 0.5$.

In the first case, which corresponds to the band-like transport regime, the mobility is computed according to the Boltzmann theory in the relaxation time approximation[33]:

$$\mu = \frac{e}{k_{\mathrm{B}}T}\frac{\sum_k \nu_k^2 \tau_k e^{-E_k/k_{\mathrm{B}}T}}{\sum_k e^{-E_k/k_{\mathrm{B}}T}}, \tag{12}$$

where $\nu_k = \hbar^{-1}\partial E_k/\partial k$ is the electron velocity at state k and τ_k is the electronic relaxation time in the elastic scattering approximation. For the present e-ph model, we obtain:

$$\tau_k^{-1} = \frac{8k_{\mathrm{B}}TL\left[1 + (2c-1)\cos(2ka)\right]}{\hbar t^{(0)}\left|\sin(ka)\right|}, \tag{13}$$
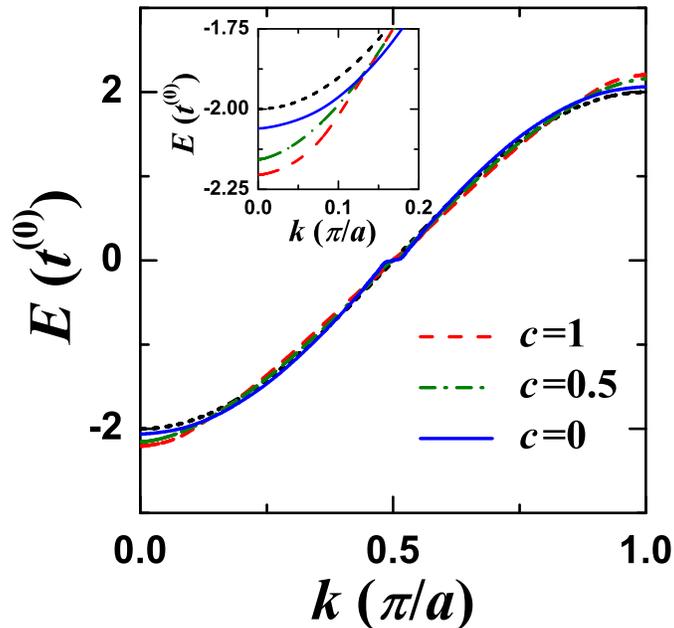
FIG. 6. (Color online) Band dispersion obtained from the maximum position of the spectral functions. All parameters are the same as in Fig. 5. The black short-dashed line is the dispersion in a perfect lattice without e-ph coupling. The inset is an enlarged view of one of the band edges.

$$\mu/\mu_0 = \frac{t_\omega^3 \hbar\omega}{32\pi L T_\omega^2 I_0 \left(t_\omega/T_\omega\right)} \int_{-1}^{1} \frac{1-x^2}{1 + (2c-1)\left(2x^2 - 1\right)} e^{-x t_\omega/T_\omega} \mathrm{d}x. \tag{14}$$

Here, $\mu_0 = ea^2/\hbar$, $t_\omega = 2t^{(0)}/\hbar\omega$, $T_\omega = k_\mathrm{B}T/\hbar\omega$ and I_0 is the modified Bessel function of the first kind.

In the second case, the mobility is computed using the Kubo formalism[34]. According to the linear response theory, the dc conductivity is given by:

$$\sigma_\mathrm{dc} = \frac{\pi\hbar}{k_\mathrm{B}TNa} \sum_{l\nu} \frac{e^{-E_\nu/k_\mathrm{B}T}}{Z} \left|\langle\varphi_l|J|\varphi_\nu\rangle\right|^2 \delta\left(E_l - E_\nu\right), \tag{15}$$

where $Z = \sum_\nu e^{-E_\nu/k_\mathrm{B}T}$ and $J = \frac{ea}{i\hbar} \sum_n t_{n,n+1}\left(a_{n+1}^\dagger a_n - h.c.\right)$. The mobility is then computed as:

$$\mu = \langle\sigma_\mathrm{dc}/en_e\rangle_{\{u_n\}}. \tag{16}$$

Here n_e is the charge density. In this study, the calculations are performed for the one-electron case (i.e., $n_e = 1/Na$).

The results derived by means of both methods are illustrated in Fig. 7. In the case of symmetric coupling, see Fig. 7a, τ vanishes at the band edges and exhibits a singularity at the band center. In contrast, in the case of antisymmetric coupling, τ exhibits singularities at the band edges and is rather constant for states within the band. When both mechanisms are contributing to the relaxation processes, $\tau(E)$ shows exactly the same trend as $\rho(E)$ and $\ell(E)$, i.e., it is essentially defined by the symmetric coupling at the band edges and by the antisymmetric coupling within the band. These characteristics of the relaxation time are reflected in the temperature dependence of the mobility, see Fig. 7b. At low temperatures when only the states near the band edge are thermally populated, the symmetric coupling mechanism leads to much lower mobilities than the antisymmetric mechanism; at high temperatures, the opposite trend is observed. Interestingly, when the e-ph interaction is dominated by the symmetric mechanism, at intermediate temperatures, the mobility exhibits a peculiar increase with temperature as a result of a crossover between two power-law ($\mu \propto T^{-n}$) regimes with different values of n at low and high temperatures. The results obtained in the framework of the Kubo formalism show similar trends, see Fig. 7c. When both mechanisms contribute to the scattering processes, a power-law-like behavior is in general observed. However, the exponent n strongly depends on the relative contributions of each mechanism and the range of considered temperatures. For instance, as seen from the inset in Fig. 7c, when only antisymmetric coupling is taken into account, the mobility show a $\mu \propto T^{-2.2}$ dependence

in the 200–400 K range, while this dependence switches to $\mu \propto T^{-1.2}$ when both mechanisms equally contribute to the overall e-ph interaction. These results point to the fact that the interplay between the two nonlocal e-ph coupling mechanisms can be an important factor responsible for the broad range of exponents n that have been measured experimentally[3,35].

VI. CONCLUSIONS

In summary, we have shown that in organic semiconductors there exist distinct symmetric and antisymmetric nonlocal e-ph coupling mechanisms that lead to different dynamical disorder patterns in real space and different coupling patterns in reciprocal space. As a result, the electronic and charge-transport properties are significantly impacted. Importantly, the symmetric and antisymmetric coupling mechanisms manifest themselves most strongly in separate situations; for instance, in the case of carrier scattering, they are most effective over different ranges of temperatures.

ACKNOWLEDGMENTS
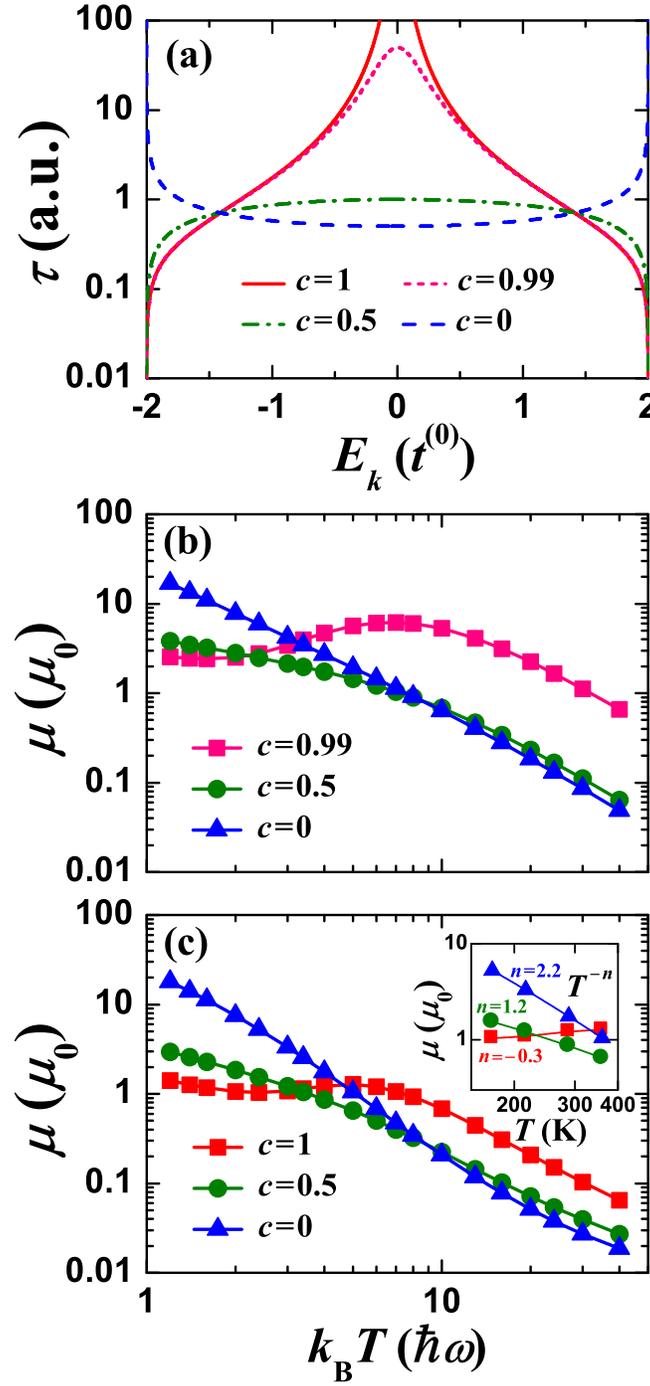
FIG. 7. (Color online) Energy-resolved electronic relaxation time (a) and electron mobility calculated by the Boltzmann theory (b) and the Kubo formula (c) as a function of the reduced temperature. All parameters are the same as in Fig. 5. In the case of Boltzmann calculations for the symmetric coupling, a value of $c = 0.99$ instead $c = 1$ is used in order to avoid the singularity shown by τ at the band center. The inset in (c) is an enlarged view near room temperature showing the power-law behavior of the mobility.

* coropceanu@gatech.edu

† jean-luc.bredas@chemistry.gatech.edu; Also affiliated with the Department of Chemistry, King Abdulaziz University, Jeddah 21589, Saudi Arabia

[1] V. Coropceanu, J. Cornil, D. A. da Silva Filho, Y. Olivier, R. Silbey, and J. L. Brédas, Chem. Rev. **107**, 926 (2007).

[2] T. Holstein, Ann. Phys. (N.Y.) **8**, 325 (1959).

[3] M. Pope and C. E. Swenberg, *Electronic Processes in Organic Crystals and Polymers*, 2nd ed. (Oxford University Press, New York, 1999).

[4] R. E. Peierls, *Quantum Theory of Solids* (Clarendon, Oxford, 1955).

[5] V. Coropceanu, M. Malagoli, D. A. da Silva Filho, N. E. Gruhn, T. G. Bill, and J. L. Brédas, Phys. Rev. Lett. **89**, 275503 (2002).

[6] N. G. Martinelli, J. Idé, R. S. Sánchez-Carrera, V. Coropceanu, J. L. Brédas, L. Ducasse, F. Castet, J. Cornil, and D. Beljonne, J. Phys. Chem. C **114**, 20678 (2010).

[7] P. Gosar and S. I. Choi, Phys. Rev. **150**, 529 (1966).

[8] R. W. Munn and R. J. Silbey, J. Chem. Phys. **83**, 1843 (1985).

[9] Y. Zhao, D. W. Brown, and K. Lindenberg, J. Chem. Phys. **100**, 2335 (1994).

[10] K. Hannewald, V. M. Stojanović, J. M. T. Schellekens, P. A. Bobbert, G. Kresse, and J. Hafner, Phys. Rev. B **69**, 075211 (2004).

[11] A. Troisi and G. Orlandi, Phys. Rev. Lett. **96**, 086601 (2006).

[12] S. Fratini and S. Ciuchi, Phys. Rev. Lett. **103**, 266601 (2009).

[13] S. Ciuchi and S. Fratini, Phys. Rev. Lett. **106**, 166403 (2011).

[14] V. Coropceanu, R. S. Sánchez-Carrera, P. Paramonov, G. M. Day, and J. L. Brédas, J. Phys. Chem. C **113**, 4679 (2009).

[15] R. S. Sánchez-Carrera, P. Paramonov, G. M. Day, V. Coropceanu, and J. L. Brédas, J. Am. Chem. Soc. **132**, 14437 (2010).

[16] A. Girlando, L. Grisanti, M. Masino, I. Bilotti, A. Brillante, R. G. Della Valle, and E. Venuti, Phys. Rev. B **82**, 035208 (2010).

[17] V. Cataudella, G. De Filippis, and C. A. Perroni, Phys. Rev. B **83**, 165203 (2011).

[18] L. J. Wang, Q. Peng, Q. K. Li, and Z. Shuai, J. Chem. Phys. **127**, 044506 (2007).

[19] D. M. Chen, J. Ye, H. J. Zhang, and Y. Zhao, J. Phys. Chem. B **115**, 5312 (2011).

[20] W. P. Su, J. R. Schrieffer, A. J. Heeger, Phys. Rev. Lett. **42**, 1698 (1979).

[21] J. Ponder, TINKER-Software Tools for Molecular Design, V. 5.1.09, (Saint Louis, 2009).

[22] D. Holmes, S. Kumaraswamy, A. J. Matzger, and K. P. C. Vollhardt, Chem. Eur. J. **5**, 3399 (1999).

[23] See supplemental materials at [ ] for more details.

[24] A. Troisi and G. Orlandi, J. Phys. Chem. A **110**, 4065 (2006).

[25] D. J. Thouless, J. Phys. C: Solid State Phys. **5**, 77 (1972).

[26] P. W. Brouwer, C. Mudry, and A. Furusaki, Phys. Rev. Lett. **84**, 2913 (2000).

[27] T. P. Eggarter and R. Riedinger, Phys. Rev. B **18**, 569 (1978).

[28] N. Koch, A. Vollmer, I. Salzmann, B. Nickel, H. Weiss, and J. P. Rabe, Phys. Rev. Lett. **96**, 156803 (2006).

[29] H. Kakuta, T. Hirahara, I. Matsuda, T. Nagao, S. Hasegawa, N. Ueno, and K. Sakamoto, Phys. Rev. Lett. **98**, 247601 (2007).

[30] S. Machida, Y. Nakayama, S. Duhm, Q. Xin, A. Funakoshi, N. Ogawa, S. Kera, N. Ueno, and H. Ishii, Phys. Rev. Lett. **104**, 156401 (2010).

[31] R. C. Hatch, D. L. Huber, and H. Höchst, Phys. Rev. Lett. **104**, 047601 (2010).

[32] J. Braun, Rep. Prog. Phys. **59**, 1267 (1996).

[33] C. Hamaguchi, *Basic Semiconductor Physics* (Springer, Berlin, 2001).

[34] G. D. Mahan, *Many-Particle Physics*, 2nd ed. (Plenum, New York, 1990).

[35] M. E. Gershenson, V. Podzorov, and A. F. Morpurgo, Rev. Mod. Phys. **78**, 973 (2006).